AMERICAN
METEOROLOGICAL
SOCIETY

Journal of Physical Oceanography

The DOI for this manuscript is doi: 10.1175/JPO-D-11-083.1

Galchenko, A., A. Babanin, D. Chalikov, I. Young, and B. Haus, 2011: Influence of wind forcing on modulation and breaking of one-dimensional deep-water wave groups. J. Phys. Oceanogr. doi:10.1175/JPO-D-11-083.1, in press.

Influence of wind forcing on modulation and breaking of one-dimensional deep-water wave groups

Alina Galchenko*, Alexander V. Babanin, Dmitry Chalikov,

Swinburne University of Technology, Melbourne, Australia

I.R. Young,

Australian National University, Canberra, Australia

Brian K. Haus

University of Miami, USA

* Corresponding author

Alina Galchenko

Swinburne University of Technology

PO Box 218

Hawthorn, Victoria, 3122

Australia

a08091985@gmail.com

Abstract

Evolution of nonlinear wave groups to breaking under wind forcing was studied by means of a fully nonlinear numerical model and in a laboratory experiment. Dependence of distance to breaking and modulation depth (height ratio of the highest and the lowest waves in a group) on wind forcing was described. It was shown that in the presence of a certain wind forcing both distance to breaking and modulation depth decrease, the latter signifies slowing down of the instability growth. It was also shown that wind forcing significantly reduces the energy loss in a single breaking event.

1. Introduction

Wave breaking is of interest in oceanography because it plays an important role in exchange of energy between atmosphere and ocean, in the air-sea exchange of momentum, mass and heat. Breaking is the main sink of wave energy, it limits the wave growth. Wave breaking contributes to ocean acoustics and also it is of significant importance for ocean remote sensing, coastal engineering, navigation and other applications (see e.g. Babanin, 2009 for a review). Dissipation due to breaking is defined by breaking probability (frequency of breaking occurrence, e.g. Babanin et al., 2001, 2007a, The WISE Group, 2007) and breaking severity (energy lost in a single breaking event, e.g. Manasseh et al., 2006, Babanin, 2009, Babanin et al., 2010). The latter can vary over a very wide range (Galchenko et al., 2010).

It has been shown that there are two important characteristics of a wave group: lifetime and modulation depth (Galchenko et al, 2010). Lifetime is time between the moment the wave is created and the moment when it breaks. This parameter is used in laboratory experiments and numerical simulations, rather than in the field; however, knowing lifetime, one can estimate breaking probability. The wave modulation depth R is a height ratio of the highest H_h and the lowest H_l waves in the group: $R = H_h / H_l$ (Babanin et al., 2010). In Galchenko et al. (2010) it was shown that these parameters depend on initial primary wave steepness and ratio of initial steepnesses of the primary wave and the sideband. It was found that the severity of breaking grows with modulation depth for the values of the latter $1<R<5.5$. It was also shown that probability of breaking for wave groups with $R<2.2$ is very low.

Modulation depth is an indicator of the rate of instability growth. One of the questions discussed in terms of wave evolution and breaking is the frequency of occurrence of Benjamin-Feir instability and how often it can be the reason for breaking. Benjamin-Feir instability is not a rare event. In one-dimensional trains it is always present, even for infinitesimally small waves. In two-dimensional wave fields its activity is limited, but within the limits it is also always present. In both one-dimensional and two-dimensional cases Benjamin-Feir instability may lead to a freak wave or may result in wave breaking (there is also the third option – full recurrence of the wave train without breaking). The main factor that defines what event is the most probable is the wave steepness, as the rate of instability depends on the steepness (provided that the bandwidth in frequency and angle is the same). For low steepness, the Benjamin-Feir instability will lead a uniform wave train to an occurrence of a wave higher than average (but that wave will only be marginally higher), and then to a full recurrence of the original uniform wave train. For steep waves, the growth rate will be large and will lead to breaking. Also, there is a range of steepnesses when waves grow very high due to Benjamin-Feir instability, but do not break, and this is when freak waves are most probable. In Babanin et al. (2011b) this range was identified as ak=0.11-0.13. Freak waves, however, are rare events, while wave breaking is frequent. There are a number of other mechanisms apart from Benjamin-Feir instability that may lead to wave breaking. In deep water and in the absence of environmental forcing (or when the forcing is relatively weak), there is only one such mechanisim, and it is linear superposition. However, Babanin et al. (2010, 2011a) conclude on the basis of multiple direct and indirect evidences, that, while linear superposition is theoretically capable to lead to a breaking in the ocean, in practice it is a very rare occurrence, and the main breaking mechanism in typical oceanic conditions is the Benjamin-Feir instability.

Benjamin-Feir instability in two-dimensional wave fields has been studied by means of dynamic equations (e.g. McLean, 1982, Mori et al., 2011), phase average equations (e.g. Alber, 1978), and experimentally (Onorato et al., 2009 a,b, Waseda et al., 2009). All the studies show that it exists in two-dimensional wave fields, but within some limited range of directional spreadings. Babanin et al. (2010) suggested that this range depends on combination of the directional bandwidth and mean wave steepness – i.e. if the steepness is higher, the directional spreading can also be broader while the instability is still active. Babanin et al. (2011 a,b) have investigated this range quantitatively in a laboratory experiment in two-dimensional wave tank. They concluded that for directional spreading and wave steepness typical for oceanic conditions, Benjamin-Feir instability is still active and leads to wave breaking.

Wind forcing has many effects on the on the evolution of nonlinear wave groups to breaking. Wind affects the rate of instability growth (Trulsen and Dysthe, 1992, Waseda and Tulin, 1999, Babanin et al., 2010). Since this rate affects the wave-breaking severity, wind therefore can be an important player in the context of the breaking strength and whitecapping dissipation. The wind forcing enhances breaking probability (e.g. Hwang et al., 1989, Banner et al., 2000, Babanin et al., 2001, 2007a), but reduces the breaking severity (Babanin et al., 2010). In the coupled wind-wave system, the breaking severity, in turn, affects the wind-to-wave energy and momentum input, even if locally (Babanin et al., 2007b). It is essential to note, however, that capacity of the wind to modify the condition of breaking onset is marginal, unless the wind is very strong (Babanin, 2009, Babanin et al., 2010, Toffoli et al., 2010).

In this paper, we are pursuing two main questions that need an answer. First is how wind forcing changes the dependencies described in Galchenko et al. (2010), i.e. the behaviour of lifetime and modulation depth as functions of initial steepness and the dependence of breaking severity on modulation depth. The investigations necessary for estimating lifetime and for describing the evolution of modulation depth were conducted by means of fully-nonlinear Chalikov-Sheinin (CS) model described in Chalikov and Sheinin (2005). The CS model implemented in this study was coupled with the atmospheric boundary layer (Chalikov and Rainchik, 2011).

An important advantage of the CS wave model is that it does not have limitations on steepness and the duration of propagation, it does not accumulate numerical errors. As mentioned above, for studying wind-wave interaction CS model is coupled with wave boundary layer model (Chalikov and Rainchik, 2011). In this coupled wind-wave model, waves are the object of the modelling. Equations for the boundary layer are solved along with full potential wave equations, and the solutions for air and water are matched through the interface. The fully-nonlinear model allows describing the effects of the wave crest sharpening, which strongly increases the pressure anomalies. It is important that model works in physical rather than Fourier space. This is an apparent advantage of the model, as many processes (e.g. group effects) can be observed only in physical space. Energy input to waves is also best described in physical rather than Fourier space because of local steepness effects (e.g., Donelan et al., 2005, 2006, Babanin et al., 2007b, Savelyev et al., 2011).

The second question is how the severity of a single breaking event changes with wind forcing. As mentioned above, in response to the wind forcing, the breaking probability grows whereas the breaking severity reduces (Babanin, 2009, Galchenko et al., 2010). As a result, trend of such an important feature as the whitecapping dissipation is not apparent.

While field investigations of the breaking severity have been an active topic of research lately, there is a clear lack of studies dealing with influence of wind on the breaking severity as such. Field measurements of breaking severity are rather complicated. Several studies (e.g. Monahan, 1971, Zhao and Toba, 2001, Guan et al., 2007, Yuan et al., 2009) established a dependence between wind speed and whitecap coverage. According to these studies, in most cases whitecap coverage tends to increase with wind speed (although, data scatter is very significant). However, whitecap coverage depends not only on the breaking severity, but also on breaking probability, and the physical and chemical properties of the water (e.g. Wu, 2000, Stramska and Petelski, 2003). Thus it is impossible to estimate the breaking strength of a single event based on the information about whitecap coverage.

A few experiments, both in laboratory and in the field, have been made with the purpose of estimating the sizes and penetration depths of bubbles produced by breakers. It is supposed that larger bubbles correspond to more severe breakers (Stolte, 1992, Manasseh et al., 2006, Babanin, 2009). Most of the studies show that the size of the bubbles and depth of their penetration into the water grow with wind forcing. However, just as in case with whitecap coverage, single breaking events are not always separated. Thus, the influence of wind on breaking severity is still in need of detailed insights. In the present paper a laboratory experiment aimed at studying breaking severity of wave groups with wind forcing is described. This is the limiting case of one-dimensional (long-crested) waves, and two-dimensional issues of modulational instability, wave breaking and wind forcing have to be studied separately.

2. Benjamin-Feir instability in the presence of wind.

The wave system in question is initially assigned by a superposition of two sinusoidal signals with different amplitudes and close wavenumbers: a carrier wave with a steepness $\varepsilon_1 = a_1 k_1$ and a sideband with a steepness $\varepsilon_2 = a_2 k_2$, where a_1 and a_2

are the wave amplitudes, k_1 and k_2 are the wavenumbers. In the non-dimensional model, however, the wave amplitude is not an independent parameter, and is defined by the choice of wave steepness and wavenumber. Wavenumbers, and therefore the initial bandwidth defined as

$$\nu = \frac{2(k_2 - k_1)}{k_2 + k_1}, \tag{1}$$

in our numerical and laboratory experiments remain the same. Initial number of waves in a group is around N=7. In the nondimensional model wavenumbers do not signify any particular dimensional values of wavenumbers, only relative rather than absolute values of these numbers are important

While propagating, this wave group experiences Benjamin-Feir instability, when new sidebands grow and take energy from the carrier wave. The classical wave system of Benjamin and Feir (Benjamin and Feir, 1967) consists of three waves: a carrier wave a and two sidebands $b_\pm$. However, Benjamin-Feir instability is not the primary interest of this study. In our numerical simulations and laboratory experiments, the upper sideband b_+ (sideband with steepness ε_2) was seeded to obtain a broad range of controlled values of modulation depth R. In such a case, the second (lower) sideband is not seeded initially, but appears from the background noise. When the wave group evolves to breaking, this lower sideband continually grows, and so does the modulation depth R. The example of such growth with no wind forcing is shown in Figure 1.

Sometimes the amplitude of sideband b_- becomes higher than the carrier wave (i.e. downshifting of the spectral energy occurs). Modulation depth R decreases with the ratio of carrier wave and lower sideband a/b_-, i.e. the higher is b_-, the larger is modulation depth. In the presence of strong wind forcing, growth of b_- can be essentially impaired (Figure 2). In the Figure, the values of ratio a/b_- at the moment of one period before breaking are plotted versus wind-forcing parameter *U/c*. Here *U* is wind speed at the height of half of the wavelength $\lambda/2$ (in CS model all parameters are non-dimensional), and *c* is phase speed of the carrier wave. The Figure represents three groups with different values of initial primary wave steepness ε_1, while ratio of initial primary steepness and steepness of sideband $\varepsilon_1/\varepsilon_2$ is the same. Figure 2 shows that suppression of the lower sideband is especially strong for wind forcing *U/c*=6-8. The broadest range of a/b_- is for $\varepsilon_1 = 0.17$. It starts from 0.94 (downshifting) for *U/c*=0 and reaches maximum of 483 for *U/c*=8. The narrowest range is for $\varepsilon_1 = 0.2$. The position of maximum remains the same for all three values of steepness, and that is *U/c*=8. Thus, the position of maximum itself is independent of steepness, but “peak width” decreases with ε_1: for $\varepsilon_1 = 0.17$ ratio higher than 100 is observed for U/c=5-9, while for $\varepsilon_1 = 0.23$ it is *U/c*=7-8.

Figure 3 shows how ratio a/b_- depends on wind forcing for wave groups with the same primary wave steepness ε_1, but different $\varepsilon_1/\varepsilon_2$. In the Figure, a/b_- reaches its maximum for close values *U/c* in both cases: *U/c*=7 for $\varepsilon_1/\varepsilon_2 = 10$, and *U/c*=8 for $\varepsilon_1/\varepsilon_2 = 60$. However, values of this maximum noticeably differ: for $\varepsilon_1/\varepsilon_2 = 10$ maximum a/b_-=8.7 , and for $\varepsilon_1/\varepsilon_2 = 60$ it is 183. Thus, suppression of lower sideband by wind significantly increases when initial sideband steepness is smaller. This happens because in case of lower initial steepness the lower sideband is suppressed before any Benjamin-Feir instability can develop. As we have mentioned above, modulation depth R depends on a/b_{-}, therefore when b_{-} is suppressed by wind, modulation depth is expected to have lower values.

Suppression of Benjamin-Feir instability by the wind for initially monochromatic and modulated wave trains was shown before by a number of researchers. Bliven et al. (1986) found that wind, when imposed on a paddle-generated “unseeded” (initially monochromatic) wave train, reduces and even (in case of strong wind) suppresses the Benjamin-Feir instability. In their experiments sideband magnitude, growth rate and low-frequency perturbation components associated with the instability mechanism were reduced when the wind speed increased. The results of Bliven et al. (1986) were qualitatively confirmed by numerical simulations of Trulsen and Dysthe (1992). They used a modification of nonlinear Schrödinger equation, to which they added two source terms: action of wind and wave breaking. Simulations of Trulsen and Dysthe showed that for low winds and breaking the evolution of wave trains was quantitavely the same as for the situation with breaking but without winds, i.e. for low winds they observed downshifting of the dominant frequency and the Benjamin-Feir instability. For stronger winds the situation was different: modulational instability existed, but was significantly slowed down and delayed in time.

Another thorough investigation on the topic was carried out by Waseda and Tulin (1999). They conducted laboratory experiments with both initially monochromatic wave trains and wave groups with two “seeded” sidebands. In the paper they report that the growth rates of the sidebands were reduced for weak, and enhanced for strong wind forcing. This seems to contradict the previous results obtained by Bliven et al. (1986). However, Bliven et al. did not estimate growth rate, but reported a suppression of the sideband energy.

One of the most recent works considering the influence of wind on Benjamin-Feir instability is that by Kharif et al. (2010). Following Segur et al. (2005), who proved numerically and experimentally that viscous dissipation can bound the growth of perturbations “before nonlinearity comes into play”, Kharif et al. (2010) numerically investigated a wave system with both dissipation and wind. They found that in the presence of both dissipation and wind, the instability in a weakly nonlinear modulated wave train occurs when friction velocity is higher than some critical velocity. Critical velocity defines the minimum friction velocity induced by the wind to amplify a wave train with a certain carrier wave frequency (critical velocity increases with wavelength or decreases with frequency of the carrier wave). Kharif et al. (2010) note that “in the presence of wind and dissipation, the unstable domain shrinks for low-frequency regime: this means that young waves are more sensitive to Benjamin-Feir instability than old waves”. The research of Kharif et al. (2010) was continued by Touboul et al. (2010), where they used a two-dimensional fully-nonlinear model, and the marginal stability curve they obtained coincided with the curve obtained with the weakly nonlinear version of Kharif et al. (2010).

3. Lifetime and modulation depth as a function of wind forcing.

Above it was shown that, as a consequence of lower sideband suppression, decrease of modulation depth (as measured at the moment of one period before breaking) can be expected when wind forcing is increasing up to *U/c*=6-8. Figure 4 represents dependence of modulation depth *R* on wind forcing *U/c* for different values of initial primary wave steepness. The difference between the three panels in Figure 4 is in ratio $\varepsilon_1 / \varepsilon_2$. Comparing the three cases, one can see that modulation depth is being reduced by wind forcing more noticeably for higher ratios of primary and secondary wave steepness $\varepsilon_1/\varepsilon_2$. In the top panel $\varepsilon_1/\varepsilon_2=5$, and the decrease of modulation depth is insignificant, while for $\varepsilon_1/\varepsilon_2=10$ (medium panel) R decreases 1.5-2 times for low values of primary wave steepness at *U/c*=6 (compared to values at *U/c*=1), and then again increases. Minimum of modulation depth and further increase is especially evident for $\varepsilon_1/\varepsilon_2=40$, i.e. for smaller initial sideband steepness. An interesting fact is that lifetime repeats this trend, though approximately, and also shows a minimum and then further increase (Figure 5). The effect of increasing lifetime for extreme winds is almost absent for $\varepsilon_1/\varepsilon_2=5$ in the top panel, hardly noticeable for $\varepsilon_1/\varepsilon_2=10$, medium panel, but strongly pronounced for a higher $\varepsilon_1/\varepsilon_2=40$ in the bottom panel. The reduction of lifetime for wind forcing *U/c*=6-8 means that the probability of breaking grows, while modulation depth is close to 1 (i.e. no modulation). This, in its turn, means that for such wind forcing modulational instability is no longer a reason for breaking.

In Galchenko et al. (2010) we showed that both lifetime (distance to breaking) and modulation depth decrease with primary wave steepness. In the presence of wind, lifetime also diminishes with primary wave steepness for any value of wind forcing, which means that for the same wind forcing probability of breaking is higher for initially steeper waves (Figure 6). With the modulation depth, situation is more complicated. Whether modulation depth depends on ε_1 or not, is defined by wind forcing. For low to moderate wind forcing R depends on ε_1. For strong wind forcing (*U/c*>5) modulation depth does not depend on primary wave steepness any more (Figure 7). Apparently, such wind forcing makes the waves grow to the limiting steepness before the modulational instability can take its course. In case of *U/c*<5 the dependence of modulation depth on primary wave steepness ε_1 can be different: it can either decrease, when $\varepsilon_1/\varepsilon_2$ is high, or increase, when $\varepsilon_1/\varepsilon_2$ is low. This dependence repeats the dependence of ratio a/b_{-} on ε_1 (Figures 8 and 9). For lower ratio $\varepsilon_1/\varepsilon_2$ modulation depth decreases with ε_1 (e.g. $\varepsilon_1/\varepsilon_2 = 7$ in Figure 8), but for higher $\varepsilon_1/\varepsilon_2$ it grows (e.g. $\varepsilon_1/\varepsilon_2 = 60$ in Figure 8).

Here it is important to note that ratio of steepnesses $\varepsilon_1/\varepsilon_2$ is not the only possible parameter for describing the dynamics of nonlinear wave groups. Benjamin-Feir instability is controlled not just by nonlinearity (the decrease of $\varepsilon_1/\varepsilon_2$ corresponds to the decrease of nonlinearity), but also by dispersion, i.e. bandwidth in the system. In our previous and current laboratory experiments on the breaking severity we concentrated on controlling modulation depth immediately before the breaking, which was achieved by manipulating $\varepsilon_1/\varepsilon_2$. In the present research initial bandwidth (also initial number of waves in a group) was not varied. In the numerical simulations, we have performed an investigation on response of modulation depth to variations of bandwidth. Such dependence without wind is shown in Figure 10. The most obvious changes in modulation depth with bandwidth occur for smaller initial steepness. Figure 11 shows dependence (or, to be more precise, no certain dependence) of *R* on bandwidth for *U/c*=2 and *U/*c=4. Maximum modulation depth for *U/c*=2 is *R*=3, for *U/c*=4 is *R*=3.4, both maximums are reached for $\nu = 0.197$. Minimums are *R*=2.3 and *R*=1.8 respectively, so the difference between maximum and minimum for the range of bandwidths shown in the Figure is 0.7 for *U/c*=2 and 1.8 for *U/c*=4. In Figure 12, one can see dependence of modulation depth on ratio $\varepsilon_1/\varepsilon_2$ for different values of bandwidth for two wind forcings. For smaller wind forcing *R* is independent of $\varepsilon_1/\varepsilon_2$, for higher, *U/c*=4, it generally decreases for all values of bandwidth. We investigated influence of wind on this dependence for different values of initial steepness ε_1 and the same bandwidth $\nu = 0.145$, and found that without wind, for small winds and extreme winds such dependence does not exist, while for high winds modulation depth decreases with $\varepsilon_1 / \varepsilon_2$ (Figure 13), just as it does for other bandwidths in Figure 12.

4. Wind and breaking severity.

In Galchenko et al. (2010) we showed that in the absence of wind severity of breaking grows with modulation depth. Also, it was found that probability of breaking for wave groups with R<2.2 is very low. Here, numerical simulations (Section 3) show that wind forcing causes the decrease of modulation depth and at the same time significantly increases the probability of breaking for wave groups with 1<R<2.2: under strong wind waves break even in groups with R close to 1. This means that with wind forcing severity of breaking is expected to decrease.

This expectation was confirmed experimentally. The laboratory experiment with wind forcing was conducted in the Air-Sea Interaction Saltwater Tank (ASIST) at the Rosenstiel School of Marine and Atmospheric Science, University of Miami. The sketch of the experimental setup is shown in Figure 14. Wave groups with wind forcing were produced by a digitally controlled mechanical wave generator and a wind generator. Laser elevation gauges with cameras measured surface elevations at a rate of 250 Hz with a vertical pixel resolution of 0.2 mm as described in Savelyev et al. (2010). Camera 1 recorded initial conditions, and breaking occurred between cameras 2 and 3.

Figure 15 shows the dependence of modulation depth on primary wave steepness for two values of wind obtained numerically and experimentally. In the

Figure, numerical values for modulation depth slightly overestimate experimental values for the case of smaller wind forcing, *U/c*=2. Quasi-two-dimensionality of the experimental conditions is most probably responsible for this overestimation.

Breaking severity coefficient was defined as follows:

$$S = \frac{E_{bb} - E_{ab}}{E_{bb}}, \tag{2}$$

where E_{bb} is the wave energy before breaking, and E_{ab} is the energy after breaking. Thus, the severity coefficient S is a nondimensional parameter. By the energy we mean potential energy of the wave group:

$$E = \int_0^T \eta^2(t)dt, \tag{3}$$

where $\eta(t)$ is time series of surface elevations, T is the period of the whole group.

Figure 16 shows dependence of severity coefficient S on wind forcing *U/c*. In Figure 16, bottom panel, data obtained for a certain wind forcing is averaged. Even though the scatter of data is significant (Figure 16, top panel), one can notice that severity coefficient decreases with wind forcing. The data in the Figure are not sorted out by initial steepnesses or any other initial conditions. Sorting by the modulation depth, ranges of which are shown with different markers in Figure 16 (top panel), does not appear to improve the scatter. Overall severity, however, does decrease with wind, which is consistent with laboratory observations of Babanin et al. (2010).

Figure 17 shows how severity coefficient grows with modulation depth for two values of wind forcing. One can notice that for weaker wind forcing of *U/c*=2 (U_{10}=5 m/s) values of severity coefficients are on average somewhat higher than for stronger wind forcing *U/c*=3.8 (U_{10}=10 m/s). This could be expected from the results presented in Figure 16: severity decreases with the wind. Also, for stronger wind forcing U/c=3.8 the scatter is more noticeable than for U/c=2. The explanation of this fact follows from the influence of wind on Benjamin-Feir instability discussed in the previous Sections: for stronger winds instability plays a less important role. It can be expected that further increase of wind (i.e. extreme wind conditions) would weaken and may even cancel the dependence $S(R)$, however, this is subject to future studies.

Comparing the results of Galchenko et al. (2010) (breaking severity versus wind forcing in the absence of wind) with results of Figure 17, we can see that the range of severity coefficients in the absence of wind is much higher than in the cases with wind (Figure 18). Maximum energy loss observed in the experiment of Galchenko et al. (2010) without wind forcing (asterisks in Figure 18) was 36%, and for the experiment with wind it is 6%. Another difference between the wind and no-wind case is that there are non-zero values of energy loss for R close to 1 (i.e. for groups with practically no modulation). This means that such waves break due to reasons other than Benjamin-Feir instability, e.g. they may grow to the limiting steepness because of the direct wind forcing before this instability takes an effect.

5. Discussion and conclusions.

Progression of one-dimensional nonlinear wave groups to breaking in the presence of wind forcing was studied by means of a fully-nonlinear numerical model and experimentally. It was shown that for certain values of wind forcing Benjamin-Feir instability is significantly suppressed and modulation depth decreases, while breaking probability increases. An opposite effect is, however, observed for extreme wind forcing.

The probability of breaking for wave groups with $1<R<2.2$, being very low without wind forcing, grows sharply in the presence of wind. This means that in the presence of such wind forcing there are reasons for breaking other than Benjamin-Feir instability.

The range of breaking severity coefficients with wind forcing is much narrower than without wind forcing. Wind increases breaking probability, but decreases the severity of a single breaker.

An approximate estimation of dependence of wave energy dissipation on modulation depth can be made using the numerical and experimental data described above. Figure 19 demonstrates numerically obtained inverse lifetime (or breaking probability $1/t_l$), severity coefficient *S*, averaged from experimental data for the corresponding values of *R*, and dissipation defined as $D=(1/t_l)*S$ as functions of modulation depth *R* for two values of wind forcing. In the Figure, for *U/c*=2 dissipation decreases and reaches saturation at *R*>2.8. At the stronger wind forcing of *U/c*=3.8. the dissipation is rather constant and on average smaller than that for *U/c*=2.

ACKNOWLEDGEMENT

We would like to thank Dahai Jeong for her assistance with the laboratory experiment. A.V. Babanin and I.R. Young gratefully acknowledge financial support of the Australian Research Council and Woodside Energy Ltd through the Linkage Grant LP0883888 and of the Australian Research Council through the Discovery Grants DP1093349 and DP1093517.

Appendix 1. Maximum and minimum energy loss for different values of wind.

[Table 1 here]

Appendix 2. Fits and their accuracy.

[Table 2 here]

[Table 3 here]

[Table 4 here]

REFERENCES

Alber, I.E. 1978 The effects of randomness on the stability of two-dimensional wavetrains. *Proc. R. Soc. Lond.*, **A363**, 525-546.

Babanin, 2009: Breaking of ocean surface waves. *Acta Phys. Slovaca*, **59**, 305-535.

Babanin, A.V., I.R. Young, and M.L. Banner, 2001: Breaking probabilities for dominant surface waves on water of finite constant depth. *J. Geophys. Res.*, **C106**, 11659-11676.

Babanin, A.V., D. Chalikov, I.R. Young, and I. Savelyev, 2007a: Predicting the breaking onset of surface water waves. *Geophys. Res. Lett.*, **34**, L07605, doi:10.1029/2006GL029135, 6p.

Babanin, A.V., M.L. Banner, I.R. Young, and M.A. Donelan, 2007b: Wave follower measurements of the wind input spectral function. Part 3. Parameterization of the wind input enhancement due to wave breaking. *J. Phys. Oceanogr.*, **37**, 2764–2775.

Babanin, A.V., D. Chalikov, I.R. Young, and I. Savelyev, 2010: Numerical and laboratory investigation of breaking of steep two-dimensional waves in deep water. *J. Fluid Mech.,* **644**, 433-463.

Babanin, A.V, T. Waseda, T. Kinoshita, and A. Toffoli, 2011a: Wave breaking in directional fields. . *Phys. Oceanogr.*, **41**, 145-156

Babanin, A.V., T. Waseda, I. Shugan, H.-H. Hwung, 2011b: Modulational instability in directional wave fields and extreme wave events. *Proceedings of the ASME 2011 30th International Conference on Ocean, Offshore and Arctic Engineering OMAE2011, July 19-24, 2011, Rotterdam, The Netherlands*, 7p

Banner, M.L., A.V. Babanin, and I.R. Young, 2000: Breaking probability for dominant waves on the sea surface. *J. Phys. Oceanogr.*, **30**, 3145-3160.

Benjamin, T.B., and J.E. Feir, 1967: The disintegration of wave trains in deep water. Part 1. Theory. *J. Fluid Mech*., **27**, 417-430.

Bliven, L., N. Huang and S. Long, 1986: Experimental study of the influence of wind on Benjamin-Feir sideband instability. *J. Fluid Mech*., **162**, 237-260.

Chalikov, D. and D. Sheinin, 2005: Modelling extreme waves based on equations of potential flow with a free surface. *Computer Physics*, **210**, 247-273.

Chalikov, D. and S. Rainchik, 2011: Coupled numerical modelling of wind and waves and a theory of wave boundary layer. *Boundary Layer Meteorology*, **138**, doi 10.1007/s 10546-101-9543-7, 1-41.

Donelan, M.A., A.V. Babanin, I.R. Young, M.L. Banner and C. McCormick, 2005: Wave follower field measurements of the wind input spectral function. Part I. Measurements and calibrations. *J. Atmos. Oceanic Tech.*, **22**, 799–813.

Donelan, M.A., A.V. Babanin, I.R. Young and M.L. Banner, 2006: Wave follower measurements of the wind input spectral function. Part 2. Parameterization of the wind input. *J. Phys. Oceanogr.*, **36**, 1672-1688.

Galchenko, A., A.V. Babanin, D. Chalikov, I.R. Young, and T.W. Hsu, 2010: Modulational Instabilities and Breaking Strength for Deep-Water Wave Groups. *J. Phys. Oceanogr.*, **40**, 2313–2324.

Guan C, W. Hu, J. Sun and R. Li . 2007. The whitecap coverage model from breaking dissipation parametrizations of wind waves. *J. Geophys. Res.*, **112**, C05031, doi:10.1029/2006JC003714.

Hwang, P.A., D. Xu, and J. Wu, 1989: Breaking of wind-generated waves: breaking and characteristics. *J. Fluid Mech.*, 202, 177-200.

Kharif, C.R., R. Kraenkel, M. Manna, and R. Thomas, 2010: The modulational instability in deep water under the action of wind and dissipation. *J. Fluid Mech.*, in press.

Manasseh, R., A.V. Babanin, C. Forbes, K. Rickards, I. Bobevski, and A. Ooi, 2006: Passive acoustic determination of wave-breaking events and their severity across the spectrum. *J. Atmos. Oceanic Tech.*, **23**, 599–618.

McLean, J.W. 1982a: Instabilities of finite-amplitude gravity waves on water of finite depth. *J. Fluid Mech.*, **114,** 331-341

McLean, J.W. 1982b: Instabilities of finite-amplitude water waves. *J. Fluid Mech.*, **114,** 315-330

Melville, W.K., 1982: Instability and breaking of deep-water waves. *J. Fluid Mech*., **115**, 165-185

Monahan, E.C., 1971: Oceanic Whitecaps. *J Phys. Oceanogr*. **1**, 139-144.

Mori, N., Onorato, M. and P.A.E.M. Janssen, 2011: On the estimation of the kurtosis in directional sea states for freak wave forecasting. *J Phys. Oceanogr*. **41**, 1484-1497.

Nepf, H.M., Wu, C.H. and E.S. Chan, 1998: A comparison of two- and three-dimensional wave breaking. *J Phys. Oceanogr*. **28**, 1496-1510.

Onorato, M. Cavaleri, L., Fouques, S., Gramstad, O., Janssen, P.A.E.M., Monbaliu, J., Osborne, A.R., Pakozdi, C., Serio, M., Stansberg, C.T., Toffoli, A., and K. Trulsen, 2009a: Statistical properties of mechanically generated surface gravity waves: a laboratory experiment in a three-dimensional wave basin. *J. Fluid Mech.*, **637** 235-257

Onorato, M., Waseda, T., Toffoli, A., Cavaleri, L., Gramstad, O., Janssen, P., Kinoshita, T., Monbaui, J., Mori, N., Osborne, A.R., Serio, M., Stansberg, C.T., Tamura, H. and K. Trulsen, 2009b: "Statistical properties of directional ocean waves, the role of modulational instability in the formation of extreme events", *Physical Review Letters*, 102, 114502-1 – 114502-4.

Savelyev, I., B. K. Haus and M. A. Donelan, 2011: "Experimental study on wind-wave momentum flux in strongly forced conditions**"**, *Journal of Physical Oceanography* (in press).

Segur, H., D. Henderson, J. Carter, J. Hammack, J., C.M. Li, D. Pfeiff, and K. Socha, 2005: Stabilizing the Benjamin-Feir instability. *J. Fluid Mech*., **539**, 229-271.

Stolte, S., 1992: Wave breaking characteristics deduced from water staff measurements. Tech. Rep. FWG report FB 1992-4, Forschungsanstalt der Bendeswehr fur Wasserschall und Geophysik.

Stramska, M., and T. Petelski, 2003: Observations of oceanic whitecaps in the north polar waters of the Atlantic. *J. Geophys. Res.*, 108(C3), 3086, doi:10.1029/2002JC001321.

The WISE Group (Cavaleri, L., J.-H.G.M. Alves, F. Ardhuin, A. Babanin, M. Banner, K. Belibassakis, M. Benoit, M. Donelan, J. Groeneweg, T.H.C. Herbers, P. Hwang, P.A.E.M. Janssen, T. Janssen, I.V. Lavrenov, R. Magne, J. Monbaliu, M. Onorato, V. Polnikov, D. Resio, W.E. Rogers, A. Sheremet, J. McKee Smith, H.L. Tolman, G. van Vledder, J. Wolf, and I. Young), 2007: Wave modeling – the state of the art, *Progress in Oceanography*, 75, 603-674.

Toffoli, A., A.V. Babanin, T. Waseda, and M. Onorato, 2010: The maximum steepness of oceanic waves. *Geophys. Res. Lett.*, **37**, L05603, doi:10.1029/2009GL041771, 4p.

Touboul, J. and C. Kharif, 2010: Nonlinear evolution of the modulational instability under weak forcing and damping. *Nat. Hazards Earth Syst. Sci*., **10**, 2589-2597.

Trulsen, K. and K. Dysthe, 1992: Action of windstress and breaking on the evolution of a wavetrain. *Breaking waves*, M. Banner and R. Grimshaw, Springer-Verlag, 243-249.

Waseda, T., Kinoshita, T. and H. Tamura, 2009: Interplay of resonant and quasi-resonant interaction of the directional ocean waves. *J. Phys. Oceanogr*., **39**, 2351-2362

Waseda, T. and M Tulin, 1999: Experimental study of the stability of deep-water wave trains including wind effects. *J. Fluid Mech*., **401**, 55-84.

Wu, J., 2000: Bubbles produced by breaking waves in fresh and salt waters. *J. Phys. Oceanogr*. **30**, 1809-1813.

Wu, C.H. and H.M. Nepf, 2002: Breaking criteria and energy losses for three-dimensional wave breaking. *J. Geophys. Res.* **C107**,3177.

Yuan, Y., L. Han, F. Hua, S. Zhang, F. Qiao, Y. Yang, and C. Xia, 2009: The statistical theory of breaking entrainment depth and surface whitecap coverage of real sea waves. *J. Phys. Oceanogr.*, **39**, 143–161.

Zhao D, and Y. Toba, 2001. Dependence of whitecap coverage on wind and wind-wave properties. *J. Oceanogr.*, **57**: 603–616.

FIGURE CAPTIONS

Figure 1. Power spectral density of the carrier wave a (asterisk), upper sideband b_+ (star) and lower sideband b_- (cross) versus time (top panel). Modulation depth versus time (bottom panel). $\varepsilon_1 = 0.17$, $\varepsilon_1 / \varepsilon_2 = 16.5$, U/c=0.

Figure 2. Ratio of power spectral densities of carrier wave a and lower sideband b_- at the moment of one period before breaking versus wind forcing for $\varepsilon_1 = 0.17$, $\varepsilon_1 = 0.2$ and $\varepsilon_1 = 0.23$, $\varepsilon_1 / \varepsilon_2 = 60$.

Figure 3. Ratio of power spectral densities of carrier wave a and lower sideband b_- versus wind forcing for $\varepsilon_1 = 0.2$, $\varepsilon_1 / \varepsilon_2 = 10$ (left) and $\varepsilon_1 / \varepsilon_2 = 60$ (right).

Figure 4. Modulation depth R as a function of wind forcing for $\varepsilon_1 = 0.17$ (asterisks), $\varepsilon_1 = 0.19$ (circles), $\varepsilon_1 = 0.21$ (squares), $\varepsilon_1 = 0.23$ (diamonds), $\varepsilon_1 = 0.25$ (pluses), $\varepsilon_1 / \varepsilon_2 = 5$ (top panel) $\varepsilon_1 / \varepsilon_2 = 10$ (medium panel), $\varepsilon_1 / \varepsilon_2 = 40$ (bottom panel).

Figure 5. Lifetime t_l in periods as a function of wind forcing for $\varepsilon_1 = 0.17$ (asterisks), $\varepsilon_1 = 0.19$ (circles), $\varepsilon_1 = 0.21$ (squares), $\varepsilon_1 = 0.23$ (diamonds), $\varepsilon_1 = 0.25$ (pluses), $\varepsilon_1 / \varepsilon_2 = 5$ (top panel) $\varepsilon_1 / \varepsilon_2 = 10$ (medium panel), $\varepsilon_1 / \varepsilon_2 = 40$ (bottom panel).

Figure 6. Lifetime t_l versus initial primary wave steepness ε_1 for three values of wind forcing: *U/c*=2 (circles), *U/c*=5 (diamonds), *U/c*=8 (squares), $\varepsilon_1 / \varepsilon_2 = 7$.

Figure 7. Modulation depth R versus initial primary wave steepness ε_1 for three values of wind forcing: *U/c*=2 (circles), *U/c*=5 (diamonds), *U/c*=8 (squares), $\varepsilon_1 / \varepsilon_2 = 7$.

Figure 8. Modulation depth as a function of initial primary wave steepness ε_1. *U/c*=4. $\varepsilon_1/\varepsilon_2 = 7$ (crosses), $\varepsilon_1/\varepsilon_2 = 20$ (circles), $\varepsilon_1/\varepsilon_2 = 40$ (pluses), $\varepsilon_1/\varepsilon_2 = 60$ (squares). Straight lines are linear fits: $\varepsilon_1/\varepsilon_2 = 7$ (solid), $\varepsilon_1/\varepsilon_2 = 20$ (dots), $\varepsilon_1/\varepsilon_2 = 40$ (dash-dots), $\varepsilon_1/\varepsilon_2 = 60$ (dash).

Figure 9. Ratio of amplitudes of carrier wave *a* and lower sideband b_- versus initial primary wave steepness ε_1. *U/c*=4. $\varepsilon_1/\varepsilon_2 = 7$ (crosses), $\varepsilon_1/\varepsilon_2 = 20$ (circles), $\varepsilon_1/\varepsilon_2 = 40$ (pluses), $\varepsilon_1/\varepsilon_2 = 60$ (squares).

Figure 10. Modulation depth versus bandwidth for $\varepsilon_1/\varepsilon_2 = 40$ (top panel) and $\varepsilon_1/\varepsilon_2 = 7$ (bottom panel), $\varepsilon_1 = 0.18$ (circles), $\varepsilon_1 = 0.21$ (squares), $\varepsilon_1 = 0.24$ (diamonds).

Figure 11. Modulation depth versus bandwidth for *U/c*=2 (diamonds), *U/c*=4 (squares). $\varepsilon_1 = 0.21$, $\varepsilon_1/\varepsilon_2 = 7$.

Figure 12. Modulation depth versus ratio of steepnesses $\varepsilon_1/\varepsilon_2$. *U/c*=2 (top panel), *U/c*=4 (bottom panel). $\nu = 0.0606$ (circles), $\nu = 0.145$ (squares), $\nu = 0.222$ (diamonds).

Figure 13. Modulation depth as a function of ratio $\varepsilon_1/\varepsilon_2$ for $\varepsilon_1 = 0.15$ (dots), $\varepsilon_1 = 0.17$ (pluses), $\varepsilon_1 = 0.19$ (circles), $\varepsilon_1 = 0.21$ (diamonds), $\varepsilon_1 = 0.23$ (squares), $\varepsilon_1 = 0.25$ (asterisks). No wind *U/c*=0 (first panel), *U/c*=4 (second panel), *U/c*=8 (third panel), *U/c*=11 (fourth panel).

Figure 14. Experimental setup scheme. Proportions are arbitrary. The distance from the wavemaker to cameras 2 and 3 is 9.15 m and 10.65 m respectively.

Figure 15. Modulation depth versus primary wave steepness for *U/c*=2 (top panel), *U/c*=3.8 (bottom panel), numerical data (stars), experimental data (circles), $\varepsilon_1/\varepsilon_2 \approx 7$.

Figure 16. Breaking severity as a function of wind forcing. Top panel: $R<2.3$ (circles), $2.3<R<2.7$ (squares), $R>2.7$ (diamonds). Bottom panel: Same, but averaged for every value of wind forcing. Laboratory observations.

Figure 17. Breaking severity versus modulation depth in the presence of wind forcing $U/c=2$ (squares), $U/c=3.8$ (stars). Laboratory observations.

Figure 18. Breaking severity versus modulation depth for $U/c=0$ (asterisks), $U/c=2$ (squares), $U/c=3.8$ (stars). Laboratory observations.

Figure 19. Breaking probability (top panel), severity coefficient (medium panel), and dissipation (bottom panel) versus modulation depth in the presence of wind. $U/c=2$ (circles), $U/c=3.8$ (squares).

CAPTIONED FIGURES AND TABLES

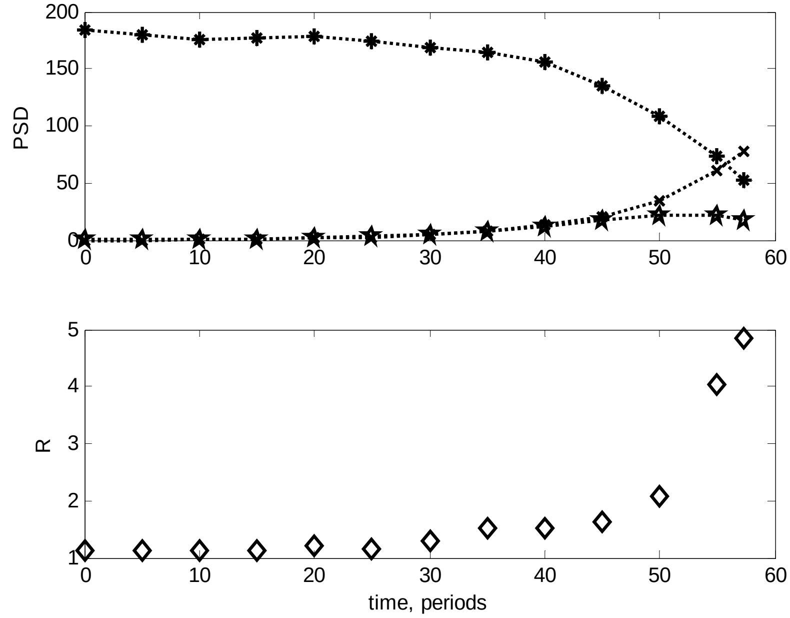

Figure 1. Power spectral density of the carrier wave *a* (asterisk), upper sideband b_+ (star) and lower sideband b_- (cross) versus time (top panel). Modulation depth versus time (bottom panel). $\varepsilon_1 = 0.17$, $\varepsilon_1 / \varepsilon_2 = 16.5$, *U/c*=0.

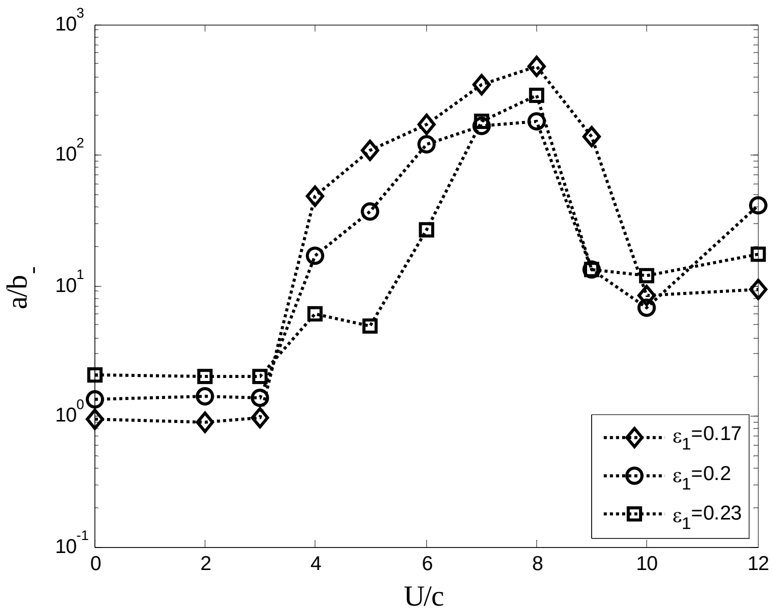

Figure 2. Ratio of power spectral densities of carrier wave *a* and lower sideband b_- at the moment of one period before breaking versus wind forcing for $\varepsilon_1 = 0.17$, $\varepsilon_1 = 0.2$ and $\varepsilon_1 = 0.23$, $\varepsilon_1 / \varepsilon_2 = 60$.

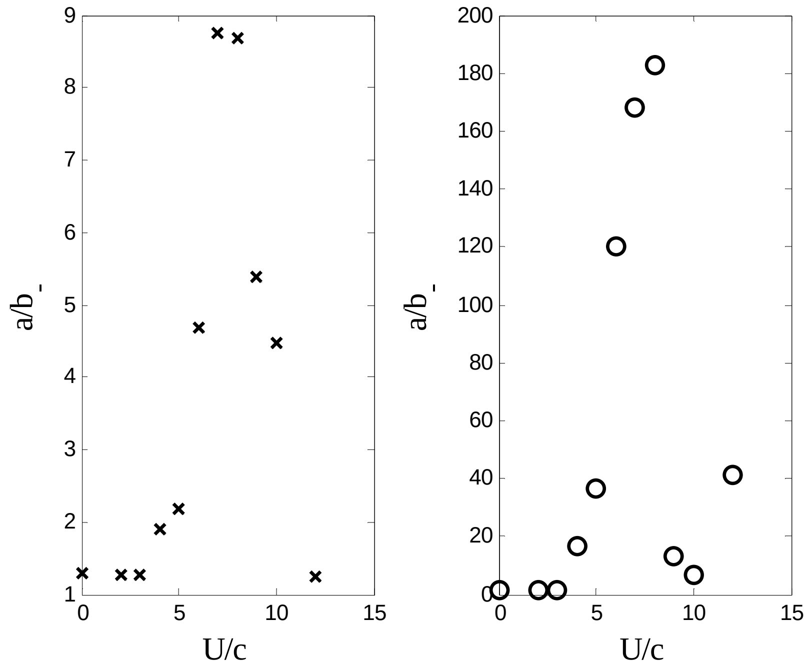

Figure 3. Ratio of power spectral densities of carrier wave a and lower sideband b_- versus wind forcing for $\varepsilon_1 = 0.2$, $\varepsilon_1 / \varepsilon_2 = 10$ (left) and $\varepsilon_1 / \varepsilon_2 = 60$ (right).

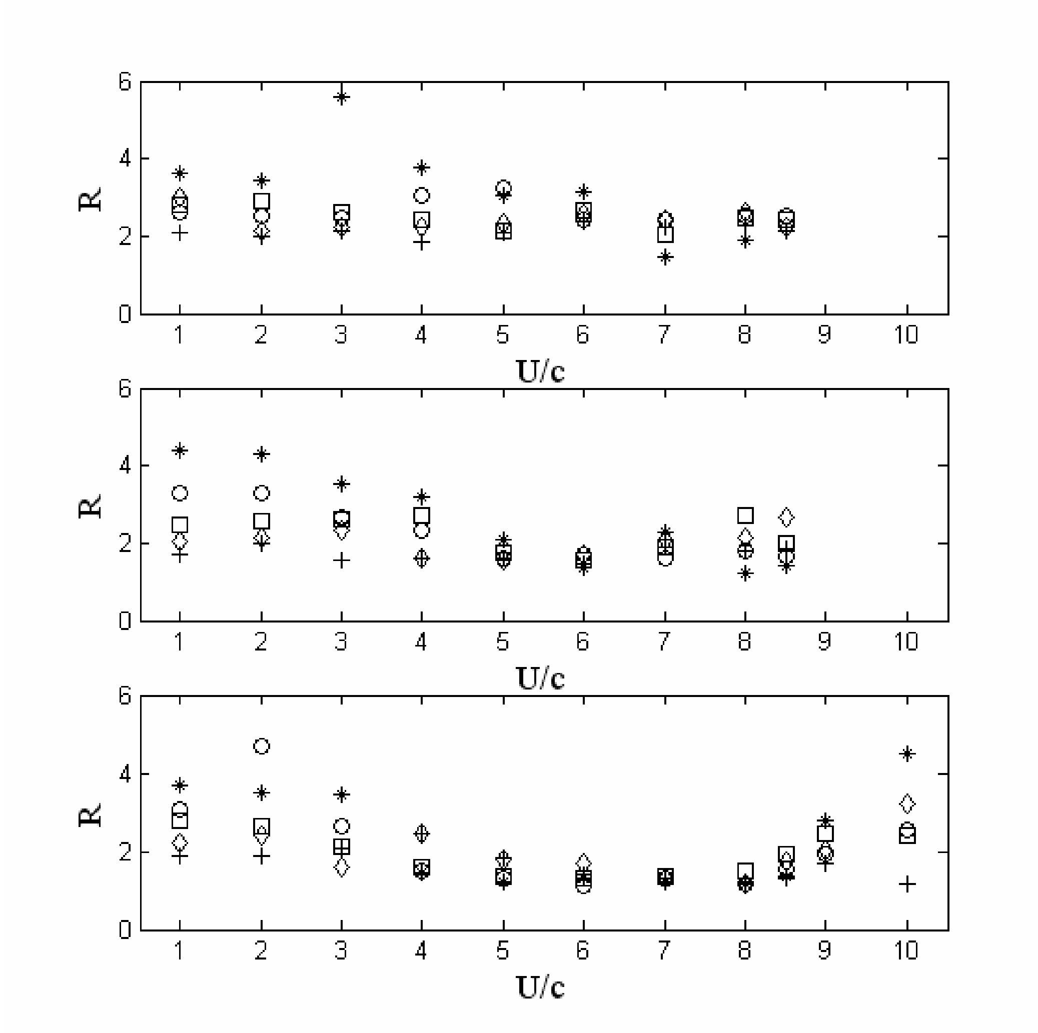

Figure 4. Modulation depth R as a function of wind forcing for $\varepsilon_1 = 0.17$ (asterisks), $\varepsilon_1 = 0.19$ (circles), $\varepsilon_1 = 0.21$ (squares), $\varepsilon_1 = 0.23$ (diamonds), $\varepsilon_1 = 0.25$ (pluses), $\varepsilon_1 / \varepsilon_2 = 5$ (top panel) $\varepsilon_1 / \varepsilon_2 = 10$ (medium panel), $\varepsilon_1 / \varepsilon_2 = 40$ (bottom panel).

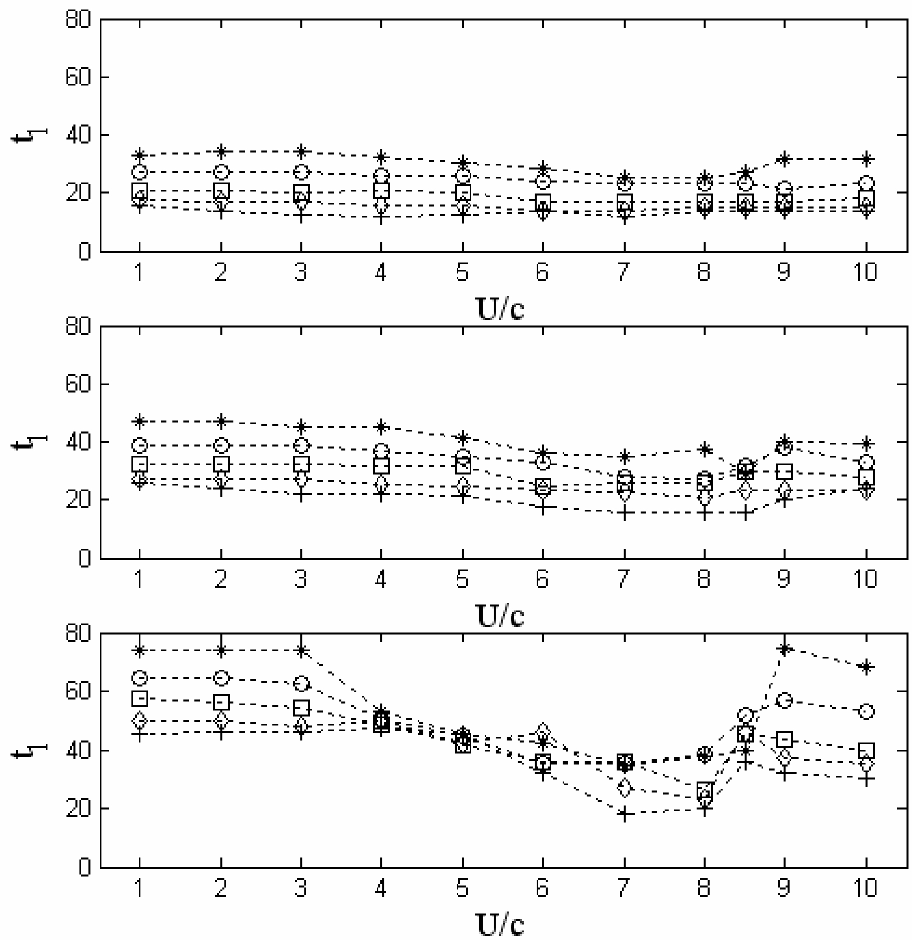

Figure 5. Lifetime t_l in periods as a function of wind forcing for $\varepsilon_1 = 0.17$ (asterisks), $\varepsilon_1 = 0.19$ (circles), $\varepsilon_1 = 0.21$ (squares), $\varepsilon_1 = 0.23$ (diamonds), $\varepsilon_1 = 0.25$ (pluses), $\varepsilon_1 / \varepsilon_2 = 5$ (top panel) $\varepsilon_1 / \varepsilon_2 = 10$ (medium panel), $\varepsilon_1 / \varepsilon_2 = 40$ (bottom panel).

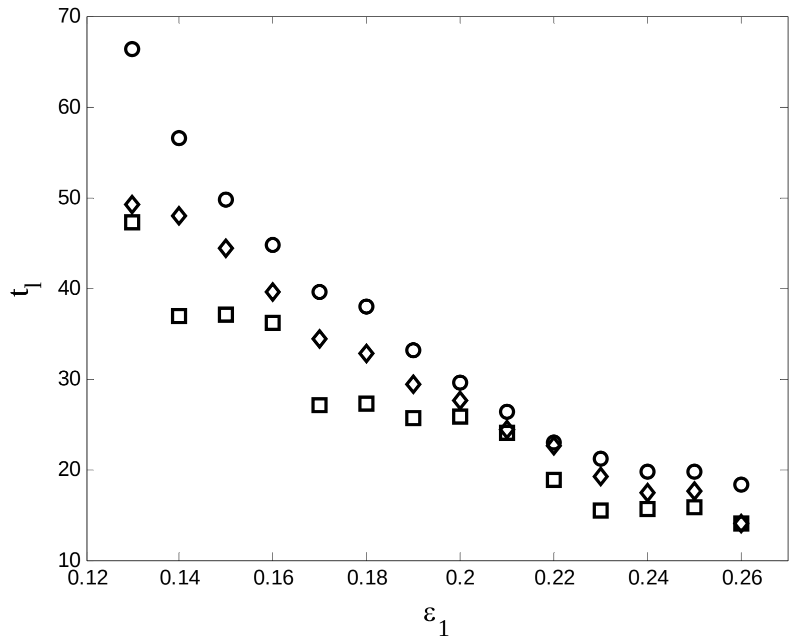

Figure 6. Lifetime t_l versus initial primary wave steepness ε_1 for three values of wind forcing: *U/c*=2 (circles), *U/c*=5 (diamonds), *U/c*=8 (squares), $\varepsilon_1 / \varepsilon_2 = 7$.

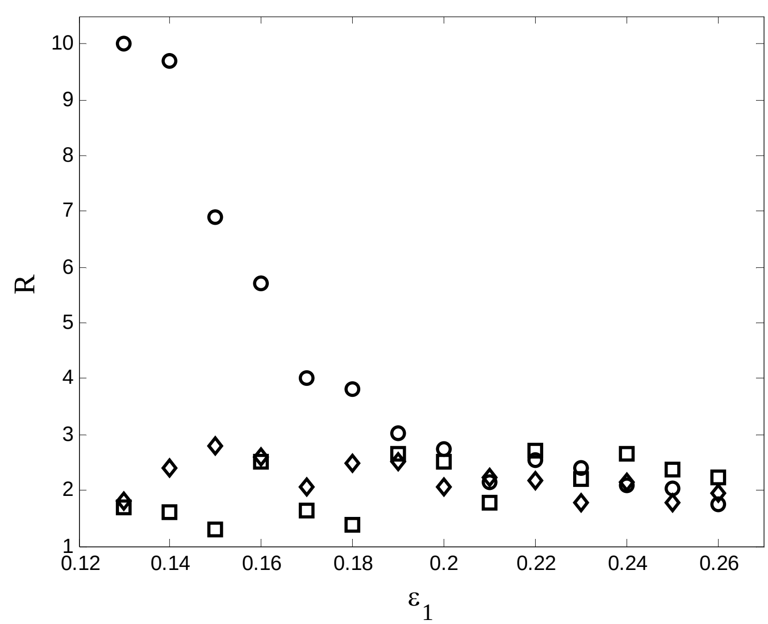

Figure 7. Modulation depth *R* versus initial primary wave steepness ε_1 for three values of wind forcing: *U/c*=2 (circles), *U/c*=5 (diamonds), *U/c*=8 (squares), $\varepsilon_1 / \varepsilon_2 = 7$.

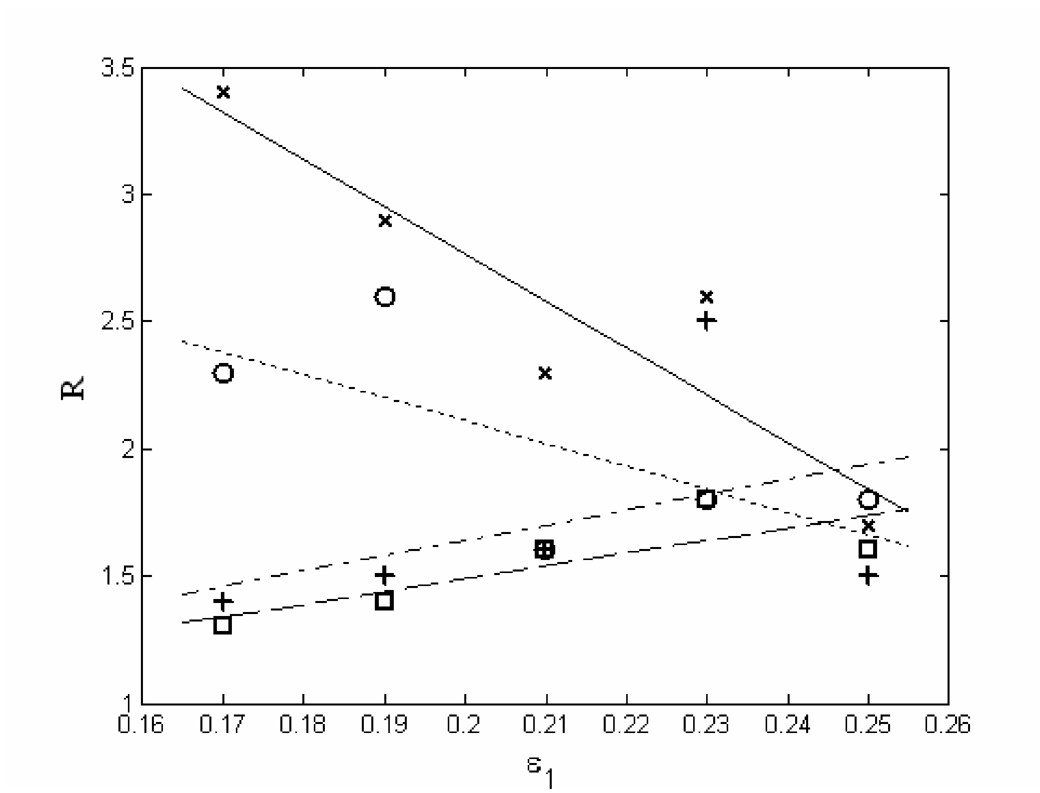

Figure 8. Modulation depth as a function of initial primary wave steepness ε_1. *U/c*=4. $\varepsilon_1/\varepsilon_2 = 7$ (crosses), $\varepsilon_1/\varepsilon_2 = 20$ (circles), $\varepsilon_1/\varepsilon_2 = 40$ (pluses), $\varepsilon_1/\varepsilon_2 = 60$ (squares). Straight lines are linear fits: $\varepsilon_1/\varepsilon_2 = 7$ (solid), $\varepsilon_1/\varepsilon_2 = 20$ (dots), $\varepsilon_1/\varepsilon_2 = 40$ (dash-dots), $\varepsilon_1/\varepsilon_2 = 60$ (dash).

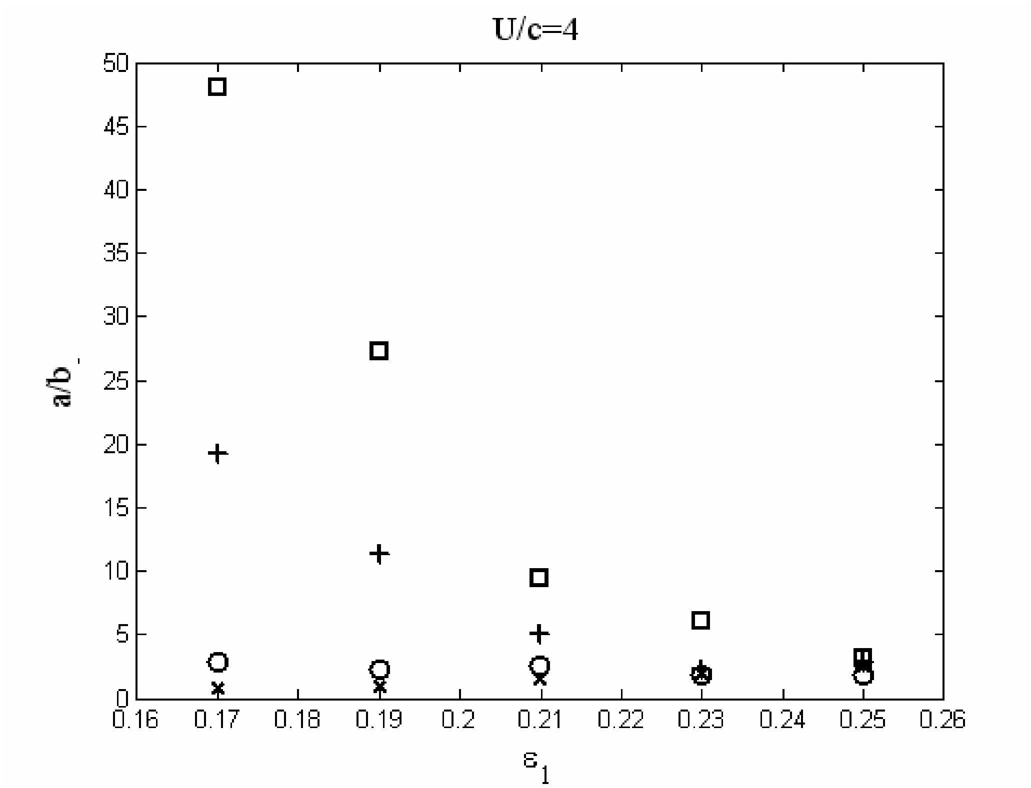

Figure 9. Ratio of amplitudes of carrier wave *a* and lower sideband b_- versus initial primary wave steepness ε_1. *U/c*=4. $\varepsilon_1/\varepsilon_2 = 7$ (crosses), $\varepsilon_1/\varepsilon_2 = 20$ (circles), $\varepsilon_1/\varepsilon_2 = 40$ (pluses), $\varepsilon_1/\varepsilon_2 = 60$ (squares).

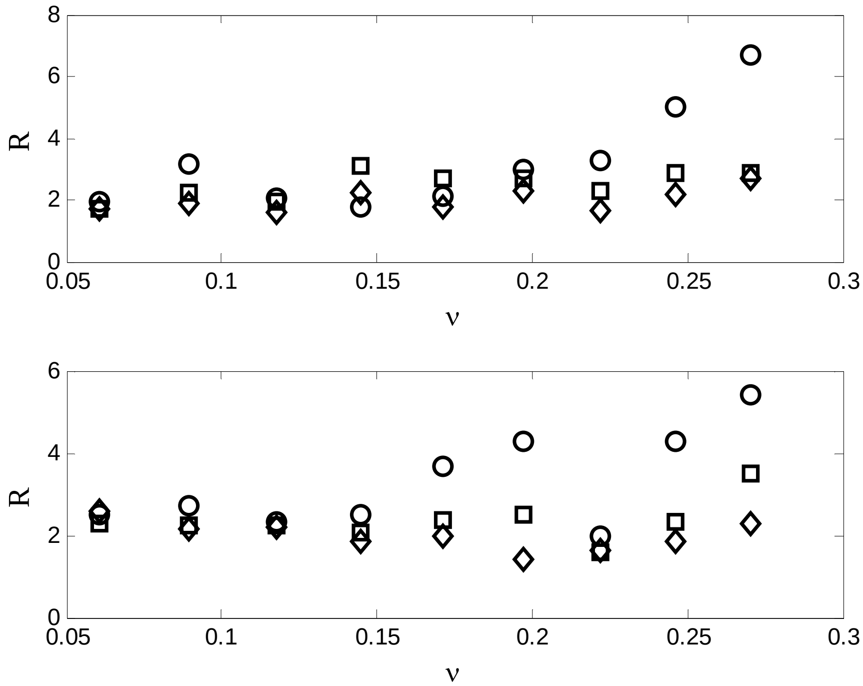

Figure 10. Modulation depth versus bandwidth for $\varepsilon_1 / \varepsilon_2 = 40$ (top panel) and $\varepsilon_1 / \varepsilon_2 = 7$ (bottom panel), $\varepsilon_1 = 0.18$ (circles), $\varepsilon_1 = 0.21$ (squares), $\varepsilon_1 = 0.24$ (diamonds).

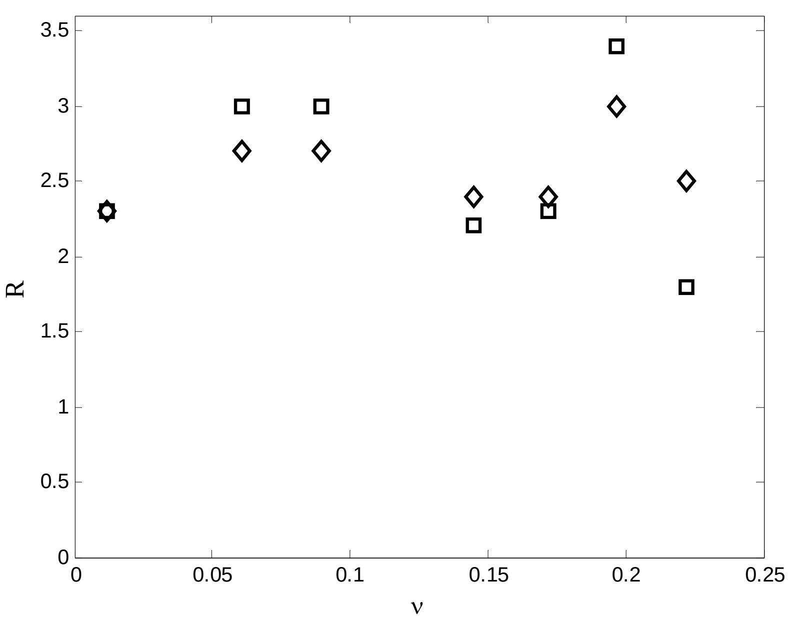

Figure 11. Modulation depth versus bandwidth for *U/c*=2 (diamonds), *U/c*=4 (squares). $\varepsilon_1 = 0.21$, $\varepsilon_1 / \varepsilon_2 = 7$.

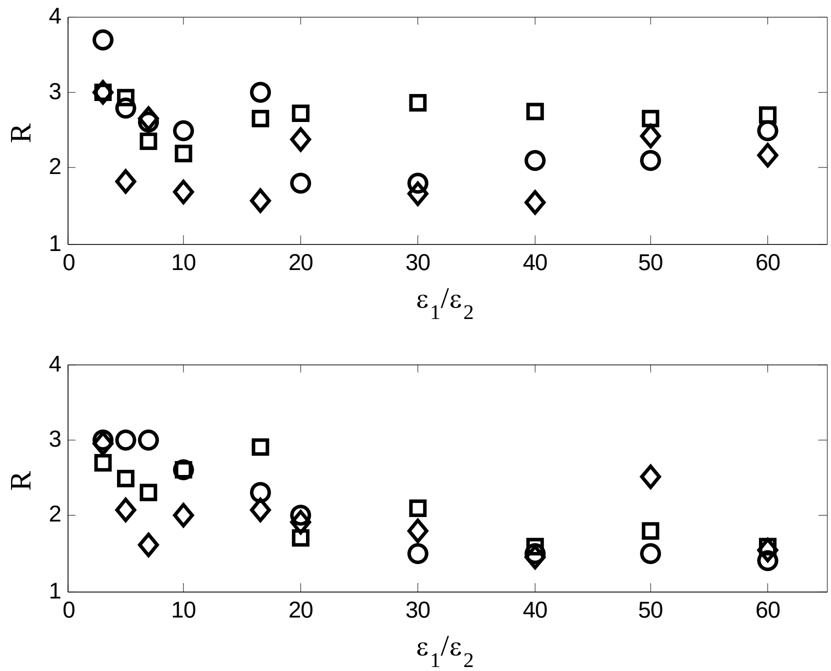

Figure 12. Modulation depth versus ratio of steepnesses $\varepsilon_1 / \varepsilon_2$. *U/c*=2 (top panel), *U/c*=4 (bottom panel). $\nu = 0.0606$ (circles), $\nu = 0.145$ (squares), $\nu = 0.222$ (diamonds).

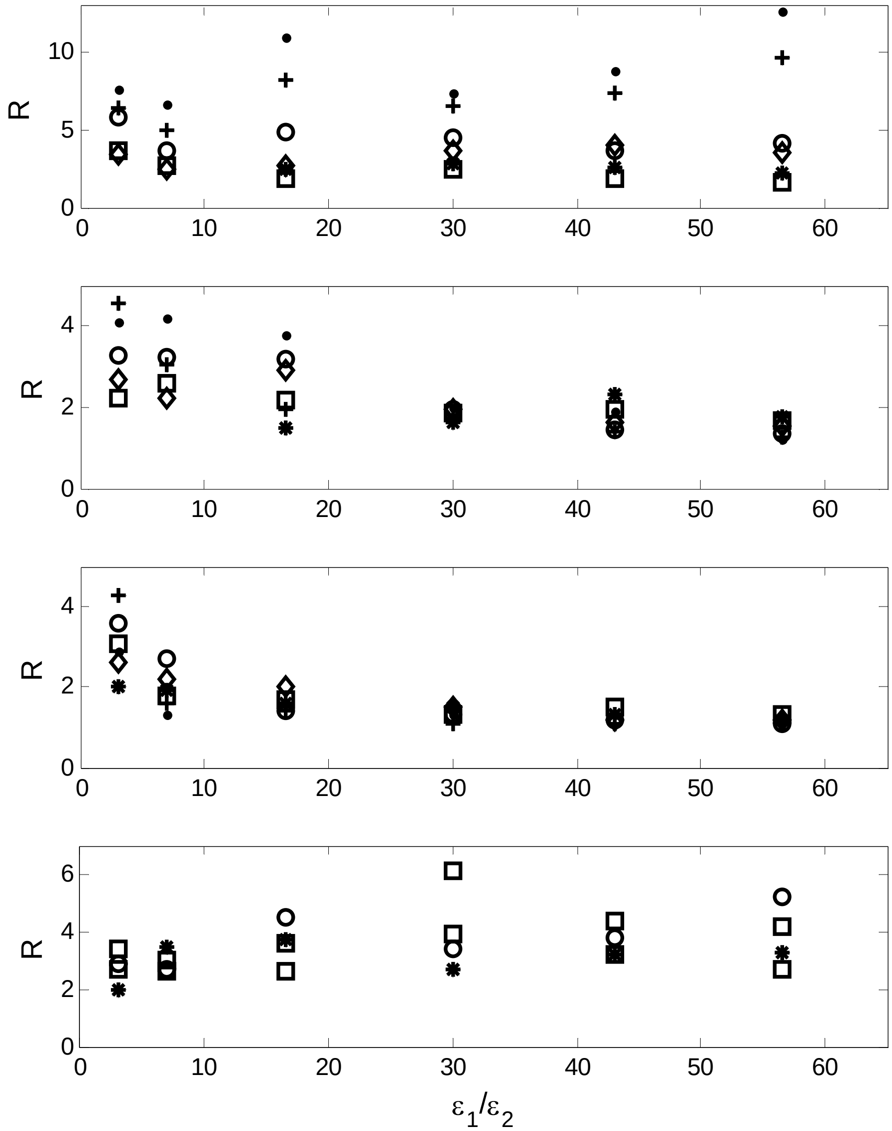

Figure 13. Modulation depth as a function of ratio $\varepsilon_1/\varepsilon_2$ for $\varepsilon_1 = 0.15$ (dots), $\varepsilon_1 = 0.17$ (pluses), $\varepsilon_1 = 0.19$ (circles), $\varepsilon_1 = 0.21$ (diamonds), $\varepsilon_1 = 0.23$ (squares), $\varepsilon_1 = 0.25$ (asterisks). No wind *U/c*=0 (first panel), *U/c*=4 (second panel), *U/c*=8 (third panel), *U/c*=11 (fourth panel).

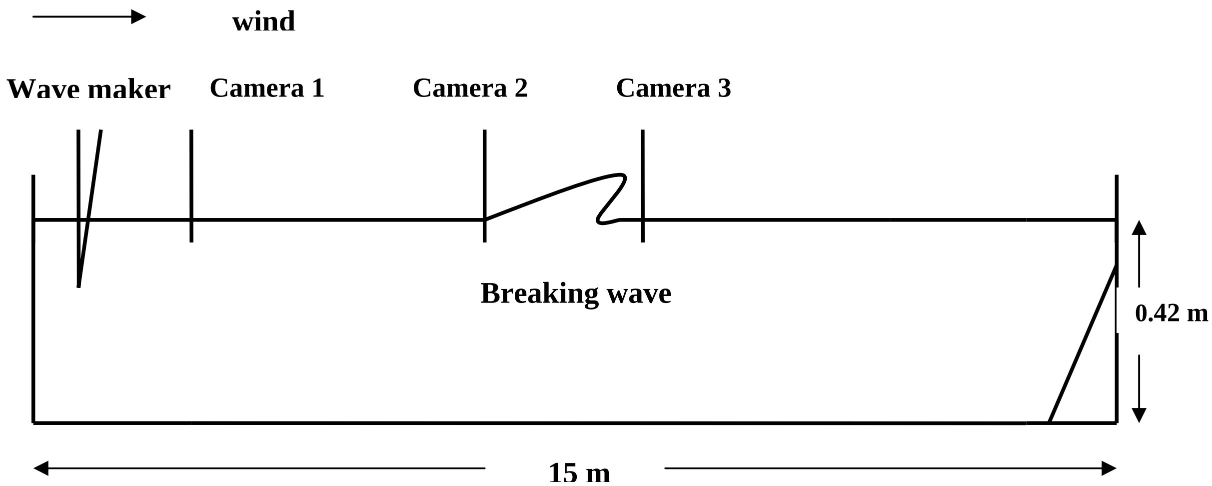

Figure 14. Experimental setup scheme. Proportions are arbitrary. The distance from the wavemaker to cameras 1, 2 and 3 is 3.3, 9.15 m and 10.65 m respectively.

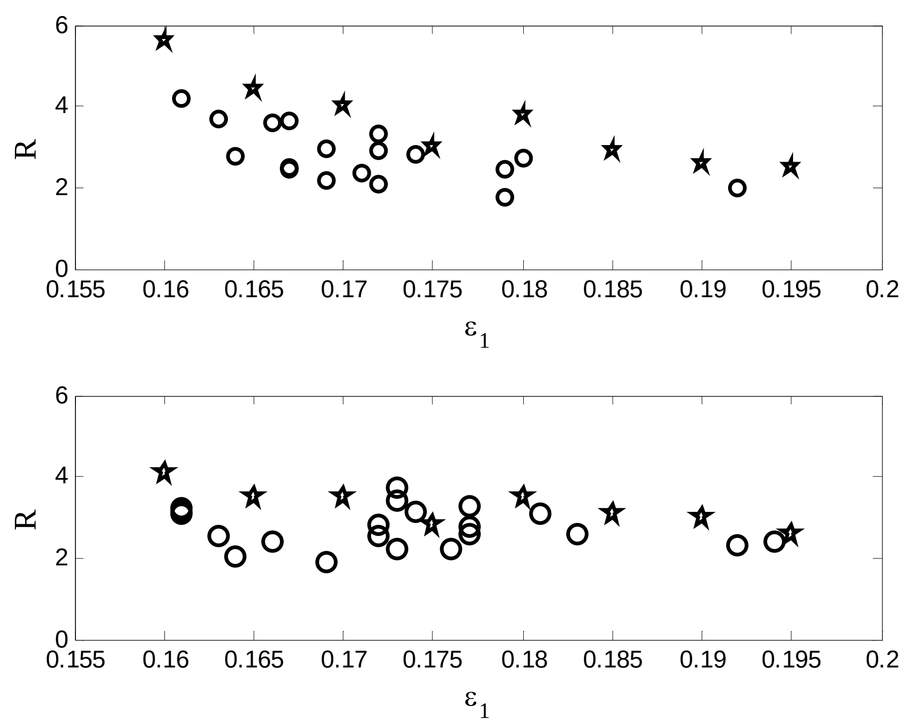

Figure 15. Modulation depth versus primary wave steepness for *U/c*=2 (top panel), *U/c*=3.8 (bottom panel), numerical data (stars), experimental data (circles), $\varepsilon_1 / \varepsilon_2 \approx 7$.

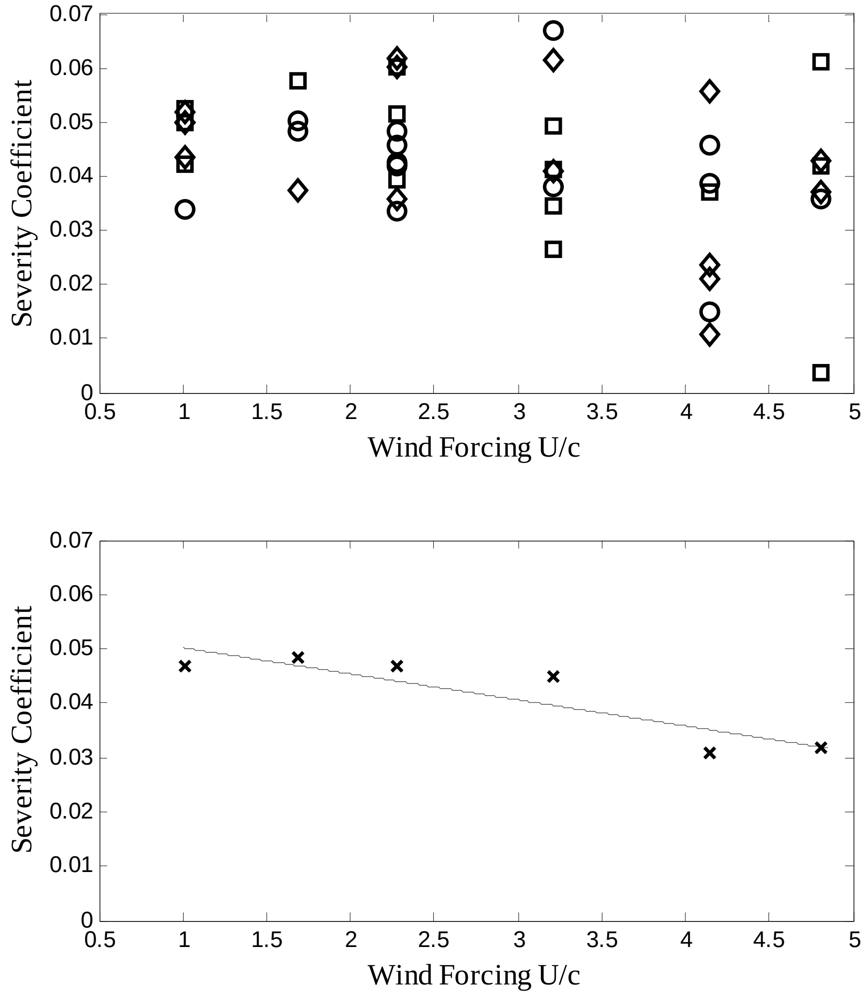

Figure 16 Breaking severity as a function of wind forcing. Top panel: *R*<2.3 (circles), 2.3<*R*<2.7 (squares), *R*>2.7 (diamonds). Bottom panel: Same, but averaged for every value of wind forcing. Laboratory observations.

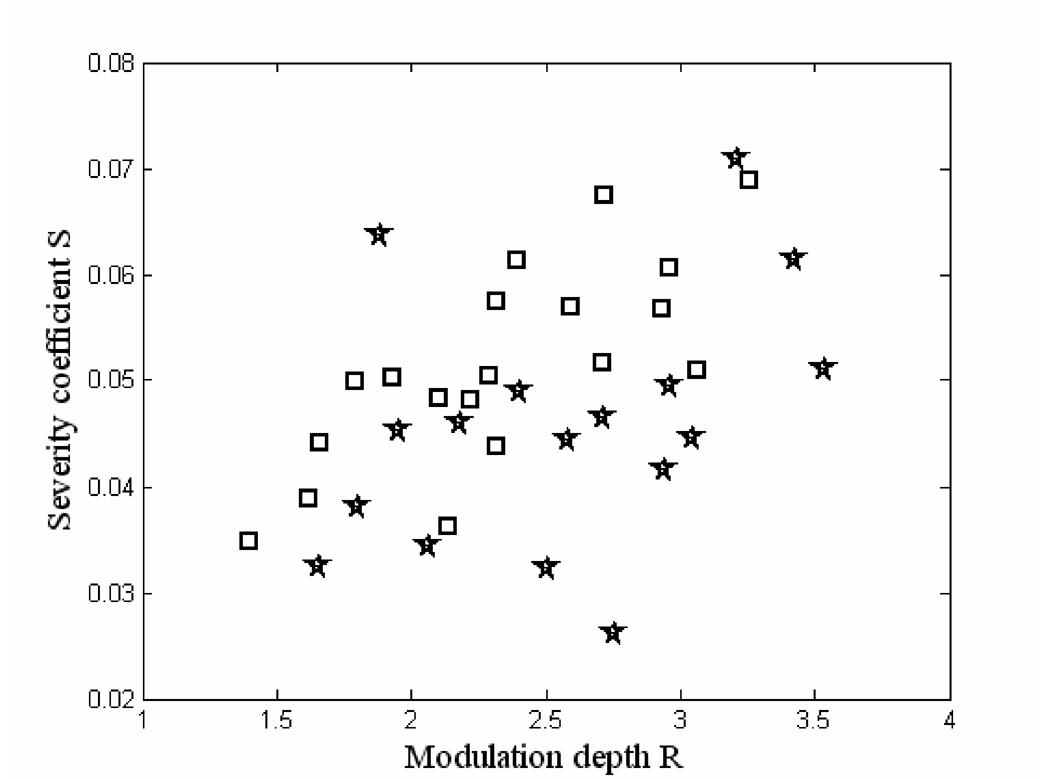

Figure 17. Breaking severity versus modulation depth in the presence of wind forcing *U/c*=2 (squares), *U/c*=3.8 (stars). Laboratory observations.

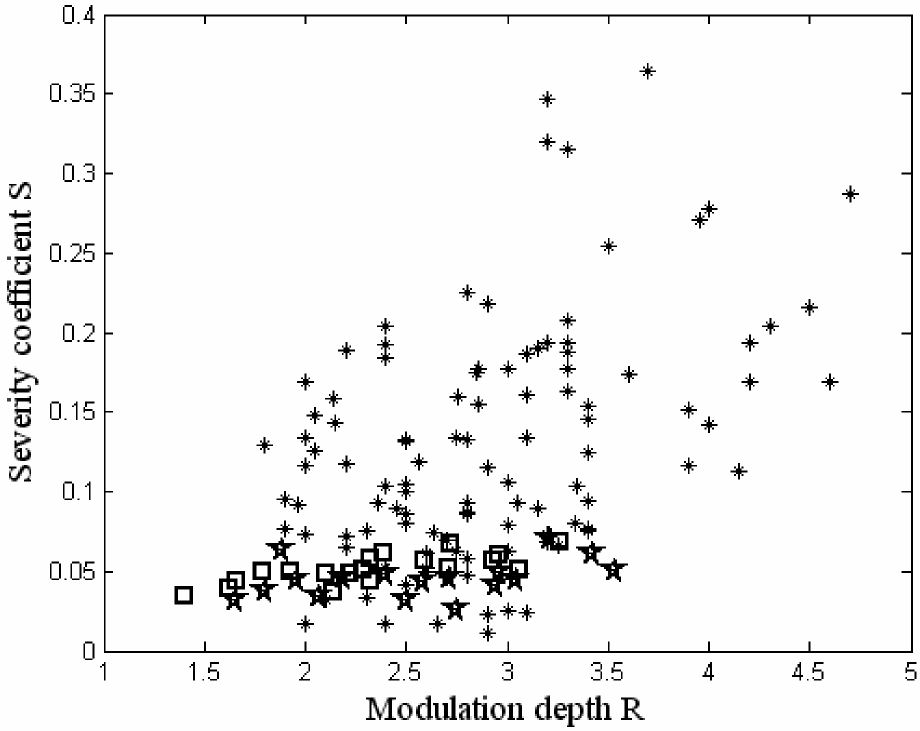

Figure 18. Breaking severity versus modulation depth for *U/c*=0 (asterisks), *U/c*=2 (squares), *U/c*=3.8 (stars). Laboratory observations.

.

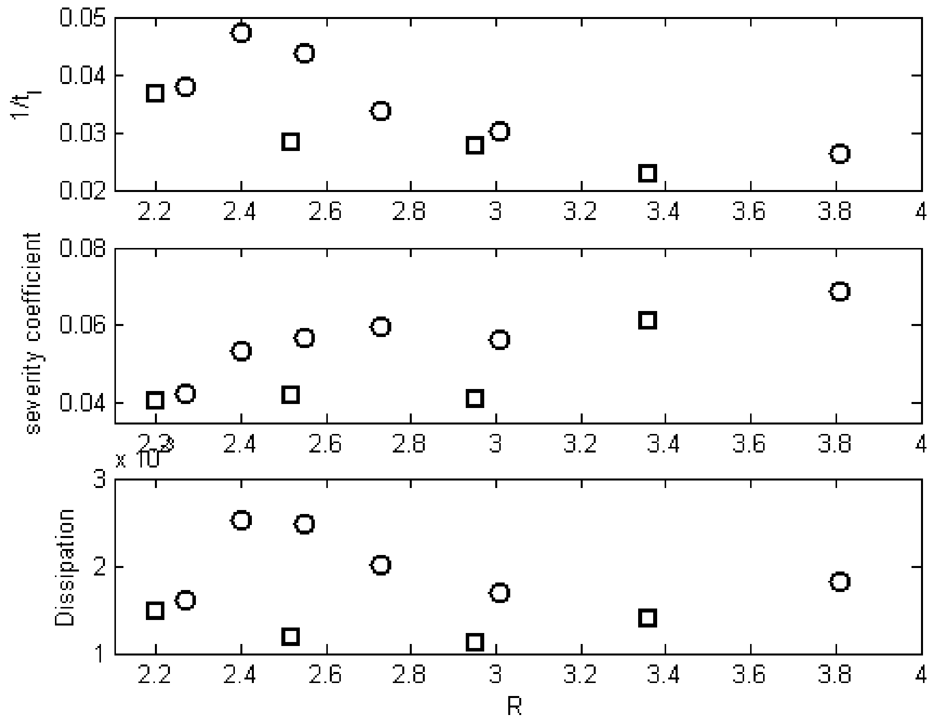

Figure 19. Breaking probability (top panel), severity coefficient (medium panel), and dissipation (bottom panel) versus modulation depth in the presence of wind. *U/c*=2 (circles), *U/c*=3.8 (squares).

U/c	$S_{\min}$ **, %**	$S_{\max}$ **, %**
0	1.1	36
2	3.5	6.9
3.8	2.6	7.1

Table1. Severity coefficients.

$\varepsilon_1 / \varepsilon_2$	**Linear fit**	**Correlation coefficient**
7	*y=-18.5x+6.5*	0.917
20	*y=-9x+3.91*	0.6862
40	*y=6x+0.44*	0.4191
60	*y=5x+0.49*	0.8111

Table 2. Correlation coefficients for Figure 8.

Linear fit	**Correlation coefficient**
y=-0.0048x+0.055	0.8894

Table 3. Correlation coefficient for Figure 11.

U/c	**Linear fit**	**Correlation coefficient**
0	*y=0.161x-0.35*	0.4378
2	*y=0.19x+0.007*	0.7564

Table 4. Correlation coefficients for Figure 13.